Astronomy & Astrophysics manuscript no. paper
November 10, 2025

Are galaxies in compact groups special?

Matthieu Tricottet[1] ⋆, Gary A. Mamon[2], and Eugenia Díaz-Giménez[3,4]

[1] 80, rue d'Alésia, 75014 Paris, France
[2] Institut d'Astrophysique de Paris (UMR 7095: CNRS & Sorbonne Université), 98 bis boulevard Arago, 75014 Paris, France
[3] CONICET. Instituto de Astronomía Teórica y Experimental (IATE), Laprida 854, X5000BGR, Córdoba, Argentina
[4] Universidad Nacional de Córdoba (UNC). Observatorio Astronómico de Córdoba (OAC), Laprida 854, X5000BGR, Córdoba, Argentina

Received XXX; accepted YYY

ABSTRACT

We investigate the properties of galaxies in compact groups (CGs) and compare them to a control sample of galaxies.

Key words. galaxies: clusters: general – catalogs

1. Introduction

2. Data

2.1. Samples

We use the compact groups and control samples we built in our previous article Tricottet et al. (2025). We nevertheless briefly recall here how they were built. Explain. Contrarily to our previous article, though, we remove CGs that we classified as *split* following Zheng & Shen (2021). In this process, our initial compact group sample of 78 groups reduced to 62.

We use the SDSS DR 16 to retrieve masses, star formation rates (SFRs) and morphologies of galaxies assessed in Galaxy Zoo Lintott et al. (2011). We specifically extracted fields `sfr_tot_p50`, `specsfr_tot_p50` and `lgm_tot_p50` from the `galSpecExtra` table, and `p_el_debiased` and `p_cs_debiased` from the `zooSpec` table.

2.2. sSFR

To build a general star formation classification that could be uniformly applied to all our samples, we extracted galaxies from the SDSS DR 16 through the query displayed in listing 1.

```
SELECT
    s.specObjID,
    s.z,
    p.petroMag_r,
    p.objID,
    g.sfr_tot_p50, g.specsfr_tot_p50, g.
        lgm_tot_p50,
    l.h_alpha_eqw, l.h_beta_eqw, l.
        oiii_5007_eqw, l.nii_6584_eqw,
    l.h_alpha_flux, l.h_beta_flux, l.
        oiii_5007_flux, l.nii_6584_flux,
    z. p_el_debiased AS p_E,
    z. p_cs_debiased     AS p_S
FROM SpecObj AS s
    JOIN PhotoObj AS p ON s.bestObjID = p
        .objID
    JOIN galSpecExtra as g ON s.specObjID
         = g.specObjID
    JOIN galSpecLine as l ON s.specObjID
        = l.specObjID
    JOIN zooSpec AS z ON s.specObjID = z.
        specObjID
WHERE s.z BETWEEN 0.005 AND 0.0452
    AND (p.petroMag_r - p.extinction_r <=
         17.77)
    AND s.class = 'GALAXY'
    AND g.lgm_tot_p50 > -1000
```

Listing 1: Query used for selecting spectral & photometric data from the SDSS

We select non-AGN galaxies by first placing them on the classical BPT diagnostic of Veilleux & Osterbrock (1987) and requiring measured values of both emission-line ratios

$$\log_{10}([\mathrm{N\,II}]\lambda6584/\mathrm{H}\alpha) \quad \text{and} \quad \log_{10}([\mathrm{O\,III}]\lambda5007/\mathrm{H}\beta).$$

A galaxy is flagged as an AGN if it satisfies either

$$\log_{10}\frac{[\mathrm{N\,II}]}{\mathrm{H}\alpha} > 0,$$

or if it lies above the empirical demarcation of Kauffmann et al. (2003):

$$\log_{10}\frac{[\mathrm{O\,III}]}{\mathrm{H}\beta} > \frac{0.61}{\log_{10}([\mathrm{N\,II}]/\mathrm{H}\alpha) - 0.05} + 1.3,$$

in which case it is removed from the non-AGN sample. All remaining galaxies—including those with missing line ratios—are retained as non-AGN. The non-AGN selection process is shown on figure 1.

We identify the galaxies having a `specsf_tot_p50` of -9999 in the SDSS as quenched (for graphic representation purposes, we give it here an arbitrary low value

⋆ matthieu.tricottet@gmail.com

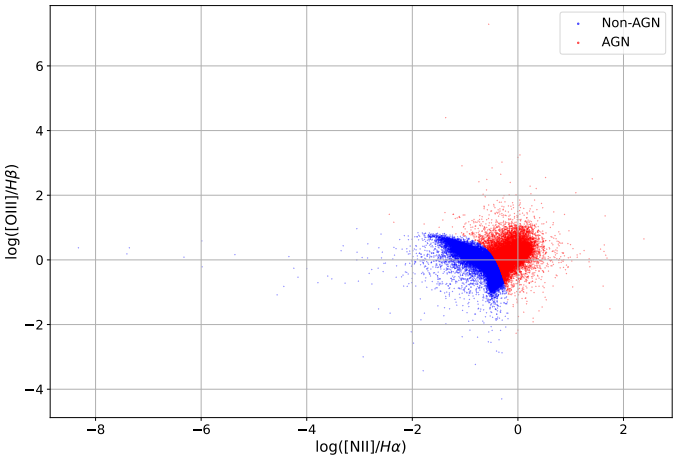

Fig. 1: BPT diagram showing our separation between ordinary and AGN galaxies

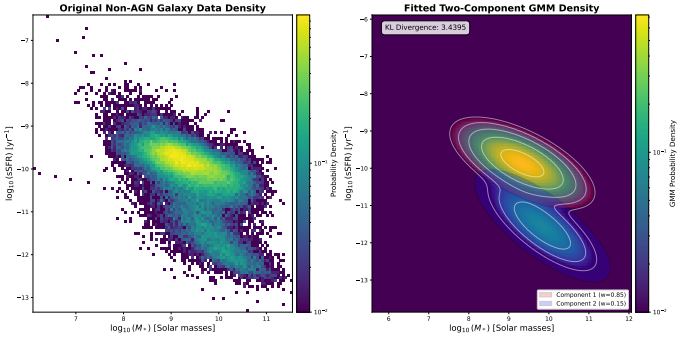

Fig. 2

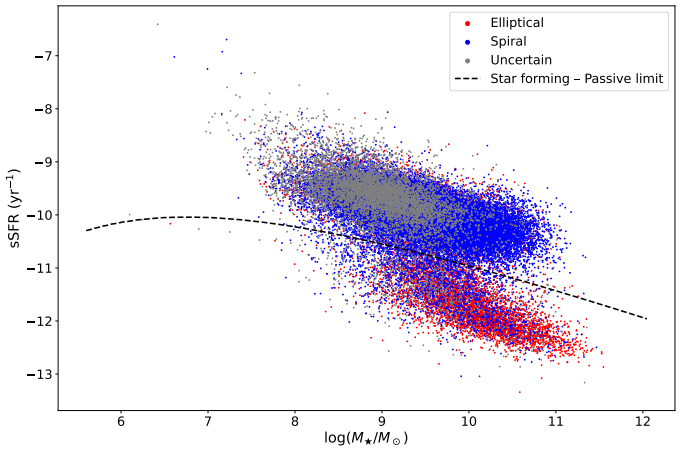

Fig. 3: sSFR vs mass, star-forming/passive limit and Zoo morphologies for the SDSS control sample, excluding quenched galaxies.

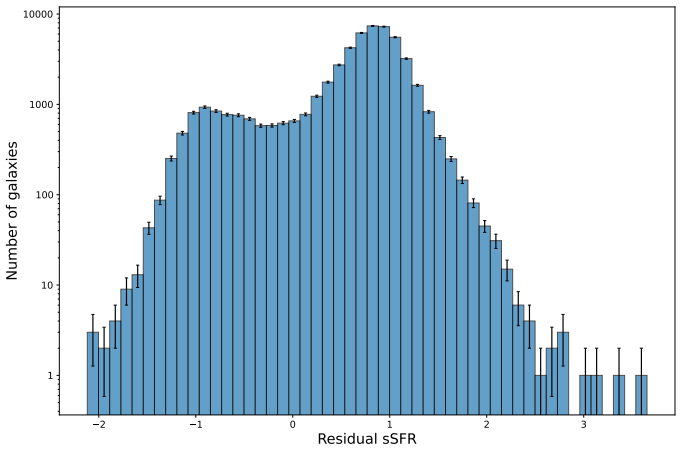

Fig. 4

of $10^{-14.0}$ Gyr^{-1}). We then consider the other ones and sort them between the star-forming and passive populations using a two-component Gaussian Mixture Model (GMM) in the $\log M_*$–$\log$ sSFR plane. Its parameters determined by minimizing the Kullback–Leibler divergence between the empirical and model densities Kullback & Leibler (1951); McLachlan & Peel (2000). For any trial parameter vector $\boldsymbol{\theta}$, we reconstruct the mixture means $\{\boldsymbol{\mu}_i\}$, covariances $\{\boldsymbol{\Sigma}_i\}$, and weights $\{w_i\}$ via a Cholesky-like decomposition and logistic mapping, optionally constraining the second component's mean to isolate the passive population Dempster et al. (1977). The KL divergence is estimated by constructing a 2D histogram of the data and summing $p_{\text{data}} \ln(p_{\text{data}}/p_{\text{GMM}})$, with a small regularization ϵ to avoid singularities Tojeiro et al. (2009); Bisigello et al. (2018). We optimize $\boldsymbol{\theta}$ via L-BFGS-B (with fallback to Nelder–Mead) over multiple guided and random initializations, selecting the solution with lowest divergence Pedregosa et al. (2011); Bishop (2006). Initial means are seeded by a median split in $\log$ sSFR to improve convergence and robustness against local minima Rousseeuw (1987). In the final fit, one component naturally aligns with the high-sSFR "star-forming sequence," while the other captures the low-sSFR "passive" cloud, providing a data-driven division that agrees with previous multi-Gaussian decompositions of the SFR–M_* plane Wuyts et al. (2011); Hahn et al. (2019). The decision boundaries, defined as the loci where the posterior probabilities of adjacent components are equal, provide an objective criterion for delineating star-forming from passive galaxies.

Add relevant GM parameters found by the algorithm.

The sSFR status for each sample is shown in table 1. Tere is no significant differences of for Star forming proportion between CG_4 and the control samples (probabilities estimated using Fisher exact test are 6.5×10^{-1} versus Control_{4B} sample, $2.5{\times}10^{-1}$ versus Control_{4C} and $1.8{\times}10^{-2}$ versus RG_4).

Restrictions of the comparison to BGGs and satellites only are also shown in table 1. The p-values found from are against Control_{4B}, against Control_{4C} and against RG_4. There is thus no significant difference in the fraction of star-forming BGGs nor satellites between CG_4 and our control samples either.

2.3. Morphology

Morphologies are determined via the Galaxy Zoo citizen-science decision tree, in which each galaxy image receives multiple independent volunteer classifications that are aggregated into debiaised vote fractions Lintott et al. (2011). Those fractions are provided in the `zooSpecz` table of the SDSS databasethrough the `p_el_debiased` and `p_cs_debiased` columns. We attribute to galaxies the morphology "elliptical" if the `p_el_debiased` value is greater

Sample		Quenched	Passive	Starforming
CG_4		18 (7.3 %)	146 (58.9 %)	84 (33.9 %)
	BGG	*(%)*	*(%)*	*(%)*
	Satellites	*(%)*	*(%)*	*(%)*
$Control_{4B}$		181 (6.5 %)	1595 (57.0 %)	1020 (36.5 %)
	BGG	*(%)*	*(%)*	*(%)*
	Satellites	*(%)*	*(%)*	*(%)*
$Control_{4C}$		191 (6.3 %)	1619 (53.8 %)	1198 (39.8 %)
	BGG	*(%)*	*(%)*	*(%)*
	Satellites	*(%)*	*(%)*	*(%)*
RG_4		5 (2.2 %)	101 (45.1 %)	118 (52.7 %)
	BGG	*(%)*	*(%)*	*(%)*
	Satellites	*(%)*	*(%)*	*(%)*
SDSS selection		*634 (1.2 %)*	*7698 (14.7 %)*	*44199 (84.1 %)*

Table 1: Number of galaxies in each sSFR status for each sample.

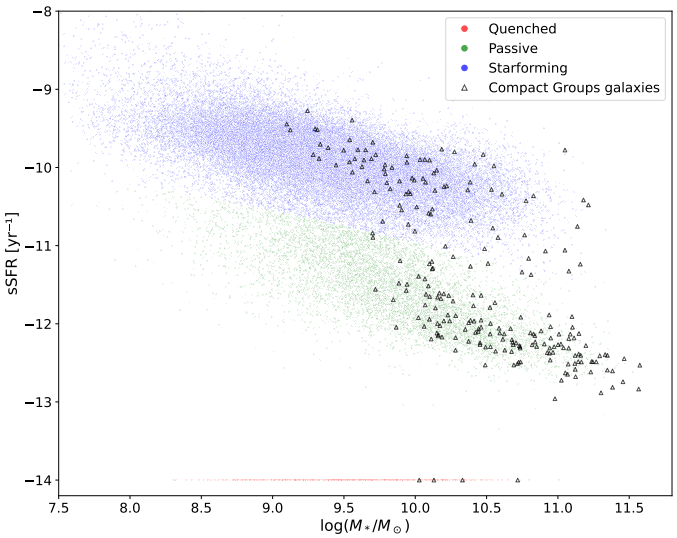

Fig. 5: sSFR and morphologies of galaxies in CG_4 and our SDSS selection. Quenched galaxies are represented at an arbitrary low value of $10^{-14.0}$ Gyr^{-1}.

than 0.5, and "spiral" if the `p_cs_debiased` value is greater than 0.5. Other cases are considered as "uncertain". The morphologies found for each sample are shown in table 2. Barnard two-sided exact tests were performed to compare the fraction of each morphology between CG_4 and each control sample. The p-values found are 5.7×10^{-5} for ellipticals and 8.5×10^{-1} for spirals versus $Control_{4B}$ sample, 2.0×10^{-1} and 1.1×10^{-1} versus $Control_{4C}$ and 1.1×10^{-3} and 3.2×10^{-3} versus RG_4. Morphologies of CG_4, wich we identified as cores of richer groups in Tricottet et al. (2025), have morphologies significantly different from ordinary groups of four members. Figure 5 displays the sSFR against masses for galaxies from the SDSS selection and for CG_4s galaxies.

2.4. Morphology vs sSFR

Starforming CG_4 are composed of 45 of their galaxies classified as spiral (84.9% once galaxies having uncertain morphology removed) and 8 (15.1% once galaxies having uncertain morphology removed) elliptical. These figures are 528 (90.4%) spiral and 56 (9.59%) elliptical galaxies for $Control_{4B}$, 671 (85.9%) spiral and 110 (14.1%) elliptical galaxies for $Control_{4C}$ and 68 (95.8%) spiral and 3 (4.23%) elliptical galaxies for RG_4. The probability that those fractions come from the same distribution is estimated from the Barnard two-sided exact test as 0.22 against $Control_{4B}$, 0.85 against $Control_{4C}$ and 4.35×10^{-2} against RG_4. There is thus neither significant excess nor lack of starforming elliptical galaxies in CG_4 compared to all our control samples.

If we restrict the comparison to BGGs only, we find 6 Elliptical BGGs (9.7% of the BGGs) and 2 Spiral BGGs (3.2%) in CG_4. This is to be compared to 71 (10.2%) Elliptical and 26 (3.7%) Spiral galaxies in $Control_{4B}$, 75 (10.0%) Elliptical and 30 (4.0%) Spiral in $Control_{4C}$, and 4 (7.1%) Elliptical and 6 (10.7%) Quenched in RG_4. The p-values found from two-sided Fisher exact test are 1.00 against $Control_{4B}$, 1.00 against $Control_{4C}$ and 0.19 against RG_4. There is thus no significant difference in the fraction of starforming BGGs between CG_4 and our control samples.

Sample	**Elliptical**	**Spiral**	**Uncertain**
CG_4	52 (21.0 %)	53 (21.4 %)	143 (57.7 %)
$Control_{4B}$	289 (10.3 %)	583 (20.9 %)	1924 (68.8 %)
$Control_{4C}$	533 (17.7 %)	781 (26.0 %)	1694 (56.3 %)
RG_4	17 (7.6 %)	75 (33.5 %)	132 (58.9 %)
SDSS selection	*10091 (19.2 %)*	*34715 (66.1 %)*	*7725 (14.7 %)*

Table 2: Number of galaxies of each morphology for each sample.

Interpolation points for sSFR classification

Acknowledgements. We thank ...

References

Hahn, C., Starkenburg, T. K., Choi, E., et al. 2019, Astrophys. J., 872
Wuyts, S., Förster Schreiber, N. M., Lutz, D., et al. 2011, Astrophys. J., 742, 96
Zheng, Y.-L. & Shen, S.-Y. 2021, ApJ, 911, 105
Bishop, C. M. 2006, Pattern Recognition and Machine Learning (Springer)
Tojeiro, R., Heavens, A. F., Jimenez, R., & Panter, B. 2009, Mon. Not. R. Astron. Soc., 397, 1263
Lintott, C., Schawinski, K., Bamford, S., et al. 2011, MNRAS, 410, 166
Kullback, S. & Leibler, R. A. 1951, Ann. Math. Statist., 22, 79
Veilleux, S. & Osterbrock, D. E. 1987, Astrophysical Journal Supplement Series, 63, 295
Dempster, A. P., Laird, N. M., & Rubin, D. B. 1977, J. R. Statist. Soc. B, 39, 1
McLachlan, G. & Peel, D. 2000, Finite Mixture Models (Wiley)
Tricottet, M., Mamon, G. A., & Díaz-Giménez, E. 2025, A&A, 699, A329
Bisigello, L., Caputi, K. I., Grogin, N., & Koekemoer, A. 2018, Astron. Astrophys., 609, A82
Kauffmann, G., Heckman, T. M., Tremonti, C., et al. 2003, Monthly Notices of the Royal Astronomical Society, 346, 1055
Pedregosa, F., Varoquaux, G., Gramfort, A., et al. 2011, J. Mach. Learn. Res., 12, 2825
Rousseeuw, P. J. 1987, Comput. Appl. Math., 20, 53